

Tautomer Selective Photochemistry in 1-(Tetrazol-5-yl)ethanol

A. Ismael,[†] M. L. S. Cristiano,[†] R. Fausto,^{*,‡} and A. Gómez-Zavaglia^{‡,§}

CCMAR and Department of Chemistry and Pharmacy, F.C.T., University of Algarve, Campus de Gambelas, 8005-039 Faro, Portugal, Department of Chemistry, University of Coimbra, Coimbra, P-3004-535, Portugal, and Centro de Investigación y Desarrollo en Criotecnología de Alimentos (Conicet La Plata, UNLP) RA-1900, Argentina

Received: September 27, 2010; Revised Manuscript Received: November 9, 2010

A combined matrix isolation FTIR and theoretical DFT/B3LYP/6-311++G(d,p) study of the molecular structure and photochemistry of 1-(tetrazol-5-yl)ethanol [1-TE] was performed. The potential energy surface landscapes of the 1*H* and 2*H* tautomers of the compound were investigated and the theoretical results were used to help characterize the conformational mixture existing in equilibrium in the gas phase prior to deposition of the matrices, as well as the conformers trapped in the latter. In the gas phase, at room temperature, the compound exists as a mixture of 12 conformers (five of the 1*H* tautomer and seven of the 2*H* tautomer). Upon deposition of the compound in an argon matrix at 10 K, only three main forms survive, because the low barriers for conformational isomerization allow extensive conformational cooling during deposition. Deposition of the matrix at 30 K led to further simplification of the conformational mixture with only one conformer of each tautomer of 1-TE surviving. These conformers correspond to the most stable forms of each tautomer, which bear different types of intramolecular H-bonds: 1*H*-I has an NH···O hydrogen bond, whereas 2*H*-I has an OH···N hydrogen bond. Upon irradiating with UV light ($\lambda > 200$ nm), a matrix containing both 1*H*-I and 2*H*-I forms, an unprecedented tautomer selective photochemistry was observed, with the 2*H* tautomeric form undergoing unimolecular decomposition to azide + hydroxypropanenitrile and the 1*H*-tautomer being photostable.

Introduction

Much attention has been paid to tetrazole (CN₄H₂) and its derivatives due to their practical importance for medicine, agriculture, petroleum industry, photography, and chemical synthesis.^{1–20} From a fundamental point of view, tetrazoles are also particularly interesting systems, especially because of the tautomerism they may exhibit and their diversified photochemistry.^{1,21–29}

Unsubstituted tetrazole, for example, was found to exist exclusively in the crystalline phases as the 1*H*-tautomer,^{30–32} whereas in solution and gas phase 1*H*- and 2*H*-tautomers coexist, the population of the most polar 1*H* form increasing with the polarity of the solvent.^{21,33–37} According to the experimental findings, 2*H*-tetrazole was found to be the lowest energy tautomer in media with a dielectric constant smaller than about 7, while in media with a larger dielectric constant, a reversal of energy takes place and 1*H*-tetrazole becomes the tautomeric ground state.^{21,38} The presence of both 1*H*- and 2*H*-tautomers of substituted tetrazoles in the gas phase has also been unequivocally proven in a series of recent studies we undertook using matrix isolation infrared spectroscopy as the main experimental technique.^{21,28} When used together with infrared spectroscopy, matrix isolation is a powerful technique for undertaking structural studies. Indeed, for a matrix-isolated compound, it is possible to achieve an essential simplification of the spectra and high spectroscopic resolution, allowing to distinguish spectral signatures of different tautomers or conformers. In addition, for matrix-isolated species, unimolecular photochemistry is expected, with the products being cage-

confined. Because molecular diffusion in the solid low temperature matrices is in general inhibited, no secondary reactions usually take place involving species resulting from different precursor molecules. Such simplification is very useful for mechanistic elucidations.

1-(Tetrazol-5-yl)-ethanol (C₃H₇N₄O; 1-TE) has been used in the design and synthesis of tetrazole-saccharinate conjugates, which receive important uses as multidentate nitrogen ligands.³⁹ The compound has the important structural characteristic of being able to establish different types of intramolecular hydrogen bonds (NH···O or OH···N), depending on the tautomeric form. In turn, these different types of intramolecular interactions can be expected to influence the chemical behavior of the tautomers. In the present study, we performed a detailed systematic study of the conformational space of the two tautomeric forms of 1-TE and investigated their photochemistries. As described in detail below, an unprecedented tautomer selective photochemistry was observed, with the 2*H*-tautomeric form undergoing prompt unimolecular decomposition when submitted to UV ($\lambda > 200$ nm) irradiation under matrix-isolation conditions, whereas the 1*H*-tautomer was found to be photostable. Matrix isolation infrared spectroscopy was used as the main experimental technique, with the experimental results receiving support from extensive quantum chemistry calculations.

Experimental and Computational Methods

Synthesis of 1-(Tetrazol-5-yl)ethanol. The synthetic route to 1-TE involved construction of the heterocycle, which was achieved by adapting the methodology developed by Sharpless and Demko.^{40,41} Sodium azide (1.43 g; 22 mmol), zinc bromide (4.50 g; 20 mmol), 2-hydroxy-propanenitrile (1.45 mL; 20 mmol), and water (50 mL) were mixed in a 250 mL round-

* To whom correspondence should be addressed. E-mail: rfausto@ci.uc.pt.

[†] University of Algarve.

[‡] University of Coimbra.

[§] Conicet La Plata, UNLP.

bottomed flask, and the mixture was stirred under reflux for 20 h. After cooling, hydrochloric acid (3 N, 30 mL) and ethyl acetate (100 mL) were added, and vigorous stirring was continued until no solid was present and the aqueous layer attained a pH of 1. The organic layer was separated and the aqueous layer extracted with ethyl acetate (2 × 50 mL). The combined organic layers were evaporated, aqueous NaOH (0.25 M; 200 mL) was added to the residue, and the mixture was stirred for 30 min until the original precipitate was dissolved and a suspension of zinc hydroxide was formed. The suspension was filtered, and the solid was washed with aqueous NaOH (1 M; 20 mL). Hydrochloric acid (3 N, 40 mL) was added to the filtrate with vigorous stirring causing the separation of an oil. After addition of a saturated solution of NaCl (brine), the aqueous layer was extracted with ethyl acetate (3 × 100 mL). The combined organic layers were dried over anhydrous sodium sulfate and evaporated to afford the final product as a white amorphous powder (1.70 g; 75% yield). IR (room temperature; KBr pellet) ν_{\max} : 3390 (OH), 1696, 1624, 1243, 1123 cm^{-1} ; ^1H NMR (CDCl_3): δ 7.55 (br, 1H), 7.22–7.35 (q, 1H), 7.35 (d, 3H); MS (EI): m/z 115 (33%; $[\text{M} + \text{H}]^+$), m/z 132 (100%; $[\text{M} + \text{NH}_4]^+$). Acc. Mass (CI): calcd for $\text{C}_3\text{H}_7\text{N}_4\text{O}$, 115.1134; found, 115.1145.

Infrared Spectroscopy and Photochemical Experiments.

The infrared (IR) spectra of 1-TE were obtained using a Mattson (Infinity 60AR Series) Fourier transform infrared spectrometer, equipped with a deuterated triglycine sulfate (DTGS) detector and a Ge/KBr beam splitter, with 0.5 cm^{-1} spectral resolution. The compound was placed in a pyrex L-shaped tube connected to a needle valve, and both sample compartment and valve nozzle were kept at about 50 °C during deposition of the matrices. Matrices were prepared by codeposition onto the cooled (10, 30 K) CsI substrate of the cryostat (APD Cryogenics closed-cycle helium refrigeration system with a DE-202A expander) of 1-TE vapors and a large excess of the matrix gas (argon N60, Air Liquide) coming from a separate line.

Irradiation of the samples was carried out with a 150 W xenon arc lamp (Osram XBO 150 W/CR OFR) through a quartz window ($\lambda > 200$ nm).

Computational Methods. The quantum chemical calculations were performed at the DFT level of theory using the standard 6-311++G(d,p) basis set⁴² and the three-parameter density functional abbreviated as B3LYP, which includes Becke's gradient exchange correction⁴³ and the Lee, Yang, Parr correlation functional.⁴⁴ Geometrical parameters were optimized using the Geometry Direct Inversion of the Invariant Subspace (GDIIIS) method.⁴⁵ Optimization of geometries was followed by calculation of the vibrational spectra at the same theory level. The nature of the obtained stationary points was checked through analysis of the corresponding Hessian matrix. Calculations were carried out using the Gaussian 03 suit of programs.⁴⁶

A set of internal coordinates was defined, and the Cartesian force constants were transformed to the internal coordinate space, allowing ordinary normal-coordinate analysis as described by Schachtneider and Mortimer.⁴⁷ These calculations were made using the program BALGA and the optimized geometries and harmonic force constants resulting from the DFT(B3LYP)/6-311++G(d,p) calculations. The calculated harmonic frequencies (scaled with the factor 0.978, which has been shown to be an appropriate choice when the theoretical level and basis set here applied are used)^{19–23} were used to assist the analysis of the experimental spectra and to account for the zero-point vibrational energy (ZPVE) corrections.

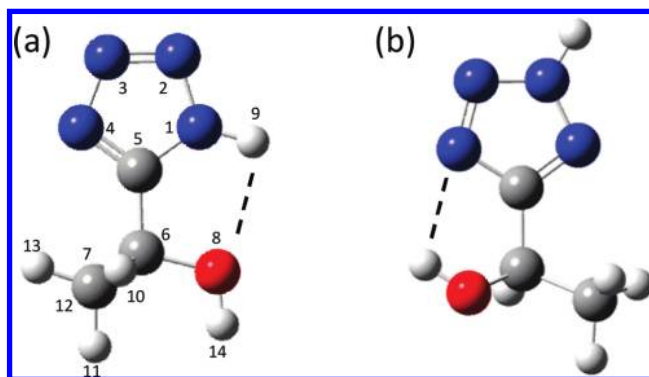


Figure 1. Most stable conformers of the two tautomeric forms of 1-(tetrazol-5-yl)ethanol and adopted atom numbering scheme: (a) 1*H*-tautomer; (b) 2*H*-tautomer. The dashed lines represent intramolecular hydrogen bonds. In the 1*H* form, $\text{N}_4\text{C}_5\text{C}_6\text{O}_8$ and $\text{C}_5\text{C}_6\text{O}_8\text{H}_{14}$ are 176.2 and 178.9 degrees, respectively; in 2*H*, these angles are -35.2 and 42.2 degrees. $\Delta E_{(1H-2H)} = 0.75$ kJ mol^{-1} .

TABLE 1: Zero Point Corrected Relative Energies ($\Delta E_0/\text{kJ mol}^{-1}$) Obtained at the DFT(B3LYP)/6-311++G(d,p) Level of Theory and Predicted Populations ($p/\%$) at Room Temperature (RT = 25 °C) and 50 °C of the Various Conformers of 1-TE^a

tautomer	conformer	ΔE_0	p (RT)	p (50 °C)
1 <i>H</i>	I	0.75	17.8	17.4
	II	3.94	4.9	5.3
	III	4.36	4.2	4.6
	IV	9.50	0.5	0.7
	V	10.12	0.4	0.5
	(all 1 <i>H</i>)		27.9	28.5
2 <i>H</i>	I	0.00	24.1	23.1
	II	0.30	21.4	20.6
	III	1.82	11.6	11.7
	IV	2.35	9.4	9.6
	V	4.28	4.3	4.7
	VI	8.73	0.7	0.9
	VII	8.87	0.7	0.8
	(all 2 <i>H</i>)		72.1	71.5

^a The conformers are depicted in Figures S1 and S2. Geometrical parameters are provided in Tables S1 and S2. The calculated total zero point corrected energy of the most stable conformer is -1082302.79 kJ mol^{-1} .

Results and Discussion

Geometries and Energies: The Potential Energy Landscape of 1-TE. 1-TE has a chiral center, the two enantiomers (*R* and *S* forms) being spectroscopically equivalent. In the present study we will focus on the *R* form. The compound may exist in two tautomeric forms (Figure 1), both having two conformationally relevant internal degrees of rotation, which are defined by the $\text{C}_5\text{--C}_6$ and $\text{C}_6\text{--O}_8$ bonds.

To identify the minimum energy conformations of 1-TE, a systematic investigation on the potential energy surface of the molecule was undertaken using the B3LYP/6-311++G(d,p) method. This search was carried out for each of the two tautomers. Table 1 displays the calculated relative energies (including zero point energy corrections) of the different conformers found. The most stable conformer of each tautomer is represented in Figure 1. The full set of conformers is shown in Figures S1 and S2 (Supporting Information); their location on bidimensional potential energy surface (PES) maps obtained by performing relaxed scans on the PES of each tautomer are shown in Figures S3 and S4 (Supporting Information). In building these maps, the $\text{C}_5\text{--C}_6\text{--O}_8\text{--H}_{14}$ and $\text{N}_4\text{--C}_5\text{--C}_6\text{--O}_8$

TABLE 2: DFT(B3LYP)/6-311++G(d,p) Calculated APT Charges (q , in Units of Electron) on Selected Atoms for the Various Conformers of 1-TE^a

tautomer	conformer	APT charges				
		q (N ₄)	q (N ₁)	q (H ₁₄)	q (H ₉)	q (O ₈)
1H	I	-0.353	-0.257	+0.267	+0.294	-0.632
	II	-0.347	-0.264	+0.256	+0.287	-0.615
	III	-0.345	-0.264	+0.257	+0.280	-0.616
	IV	-0.380	-0.273	+0.313	+0.269	-0.622
	V	-0.380	-0.273	+0.311	+0.267	-0.617
		(-0.361 ± 0.018)	(-0.266 ± 0.007)	(+0.281 ± 0.029)	(+0.279 ± 0.012)	(-0.620 ± 0.007)
2H	I	-0.300	-0.231	+0.293	+0.280	-0.625
	II	-0.296	-0.228	+0.278	+0.283	-0.627
	III	-0.281	-0.257	+0.278	+0.282	-0.613
	IV	-0.279	-0.256	+0.273	+0.281	-0.608
	V	-0.264	-0.238	+0.256	+0.279	-0.640
	VI	-0.262	-0.214	+0.245	+0.280	-0.632
	VII	-0.253	-0.219	+0.244	+0.275	-0.630
		(-0.276 ± 0.018)	(-0.235 ± 0.017)	(+0.267 ± 0.019)	(+0.280 ± 0.003)	(-0.625 ± 0.011)

^a Conformers are depicted in Figures S1 (1H forms) and S2 (2H forms). Numbers in parentheses correspond to mean ± standard deviation values.

dihedral angles were varied in increments of 30 degrees and all other geometric parameters were let free during the geometry optimization. The optimized geometries for the various conformers are given in Tables S1 and S2 (Supporting Information). On the whole, 12 conformers were found, 5 for tautomer 1H and 7 for tautomer 2H.

As expected, the calculations yield the most stable conformer of tautomer 2H as being the global minimum. However, the energy of the most stable conformer of tautomer 1H was predicted to be only 0.75 kJ mol⁻¹ higher than that of the latter species. Both tautomers have other low energy conformers: forms 2H-II, III, IV, and V and 1H-II and III have calculated relative energies to the most stable conformer of the corresponding tautomeric form smaller than 5 kJ mol⁻¹. The populations of the different conformers in gas phase at room temperature (25 °C), obtained according to the Boltzman statistics and taking into account the DFT calculated relative energies, are given in Table 1. Conformers 1H-I and 2H-I, II, III, and IV are predicted to have populations above or about 10%, while conformers 1H-II and III and 2H-V should have populations of about 5–4%. The remaining four conformers were predicted to have negligible populations at room temperature (RT). On the whole, tautomer 2H was predicted to account for about 72% of the total equilibrium population versus ~28% of tautomer 1H. Table 1 also gives the populations expected for the gas phase equilibrium at 50 °C (the temperature of the vapor of the compound used to prepare the matrices in the present study), which are equal, in practical terms, to those characteristic of the RT gas phase. In particular, one can conclude that only conformers 1H-I, II, and III and 2H-I, II, III, IV, and V might be of experimental relevance for the present study.

The relative stability of the conformers can be correlated with the dominant type of intramolecular interaction in each form. In the case of tautomer 2H, the five conformers bearing an intramolecular hydrogen bond of type OH...N correspond to the most stable forms (with relative energies below 5 kJ mol⁻¹), whereas conformers 2H-VI and VII, which do not have any intramolecular H-bond, have relative energies of about 9 kJ mol⁻¹. In the two most stable conformers (2H-I and II), the OH...N bond involves the more negatively charged N₄ atom as electron donor (see Table 2), while in 2H-III, IV, and V, the H-bond electron donor atom is N₁. The correlation found between the APT charge on H₁₄ (Figure 2) and the energy of

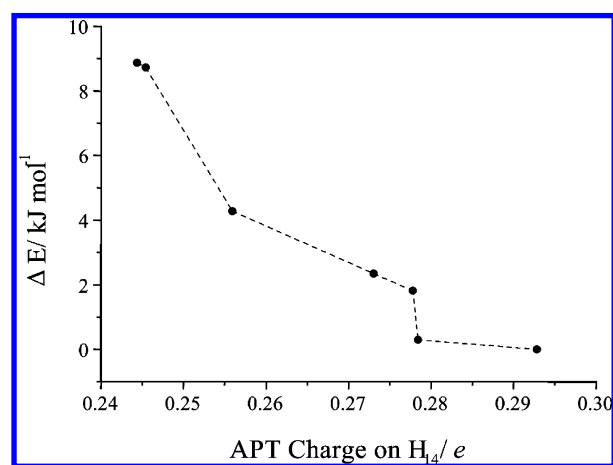


Figure 2. Relative energy (including zero point correction) of the conformers of tautomer 2H of 1-TE as a function of the calculated APT charge on the hydroxyl hydrogen atom (H₁₄). The line connecting the points is for guiding the eyes.

the 2H conformers is also a good indicator of the relevance of the intramolecular OH...N hydrogen bond to their relative stability. In the case of tautomer 1H, the three most stable conformers (1H-I, II, and III, with relative energies below 4 kJ mol⁻¹) possess an intramolecular hydrogen bond of type N-H...O. Conformers 1H-IV and V bear an H-bond of type OH...N, but they have also an important repulsive interaction between the ring hydrogen atom and the methyl and/or methine hydrogen atoms and, as a result, they have relative energies above 9 kJ mol⁻¹.

Of great relevance for the matrix isolation study undertaken in this investigation are the energy barriers separating the different conformers. It is well-known that during deposition of a cryogenic matrix conformational cooling may take place if the barriers to conformational isomerization are low enough (below a few kJ mol⁻¹).^{48–50} We have shown that the extent of the observed conformational cooling depends on the temperature of the cold substrate during matrix deposition, the higher the temperature the more extended the conformational cooling.⁴⁸ The relevant barriers for conformational conversion in 1-TE were then evaluated at the DFT(B3LYP)/6-311++G(d,p) level of theory. The results obtained for the 1H tautomer clearly indicate that conformers 1H-II and III are separated from the most stable conformer 1H-I by energy barriers below 1 kJ mol⁻¹

(0.68 and 0.87 kJ mol⁻¹ for 1*H*-II and III, respectively) and should then convert to this latter form during matrix deposition. The higher energy forms also have very low predicted energy barriers to lower energy forms and, ultimately, shall also be converted into the most stable form. In practical terms, these results led one to expect an observation of a single conformer of tautomer 1*H* in the matrix-isolation experiments: conformer 1*H*-I. If the sublimated vapor of the compound used to prepare the matrices correspond to an equilibrium state (both regarding tautomerization and conformational interconversion) conformer 1*H*-I should correspond to a population of about 28% of the total population. For tautomer 2*H*, the calculations predict that conformer 2*H*-II should convert to conformer 2*H*-I during deposition (calculated energy barrier 1.89 kJ mol⁻¹) and conformers 2*H*-IV and V to conformer 2*H*-III. The barrier between 2*H*-III and 2*H*-I is also low, 3.95 kJ mol⁻¹, but still large enough to preclude extensive conversion of the higher energy form into the lower energy conformer during deposition at the lowest temperatures attainable in our matrix-isolation set up (10 K). The two highest energy conformers (2*H*-VI and VII) also have barriers of isomerization to lower energy conformers on the order of 4–5 kJ mol⁻¹ and may in principle also be trapped in the matrices deposited at 10 K. However, their populations in the gas phase prior to deposition are certainly below 1% and their unequivocal experimental detection looks improbable. In summary, the theoretical results point to the possibility of experimental observation of two main conformers of tautomer 2*H* in the argon matrices deposited at 10 K, conformers 2*H*-I and III and also to the eventual presence of conformers 2*H*-VI and VII in trace amounts. If the sublimated vapor of the compound used to prepare the matrices correspond to an equilibrium state both regarding tautomerization and conformational interconversion, the expected populations of conformers 2*H*-I and III should be about 45 and 25%, respectively.

Infrared Spectra of the Matrix-Isolated Compound: Selection of Conformational States. In both tautomeric forms (C₁ symmetry), 1-TE has 36 fundamental vibrations, all active in the infrared. The results of the theoretical vibrational calculations undertaken in the present investigation are presented in the Supporting Information: Tables S3 and S4 display the sets of internal coordinates used in the normal coordinate analysis performed on tautomers 1*H* and 2*H*, respectively, and Tables S5–S13 the calculated infrared spectra and potential energy distributions (PED) for the lower energy ($\Delta E < 5$ kJ mol⁻¹) conformers.

The infrared spectrum of 1-TE isolated in an argon matrix with substrate kept at 10 K during the matrix deposition is presented in Figure 3, together with the calculated spectra for the most stable conformers of each 1-TE tautomer. The spectrum resulting from the juxtaposition of the two calculated spectra is also shown in this figure. As it can be noticed, this latter spectrum nicely fits the experimentally obtained one, indicating that conformers 1*H*-I and 2*H*-I are the main contributors to the observed spectrum, as suggested by calculations. Upon annealing of the matrix to 30 K, some bands were found to vanish. These bands are observed in several spectral regions, such as, for example, that presented in Figure 4. One group of these bands fits nicely the predicted IR spectrum of conformer 2*H*-III (e.g., bands around 570 and 715 cm⁻¹ in Figure 4). As mentioned above, this conformer could also be expected to be present in the matrix deposited at 10 K with a significant population: the relatively low energy barrier for the 2*H*-III → 2*H*-I conversion, 3.95 kJ mol⁻¹, is still large enough to prevent full conversion

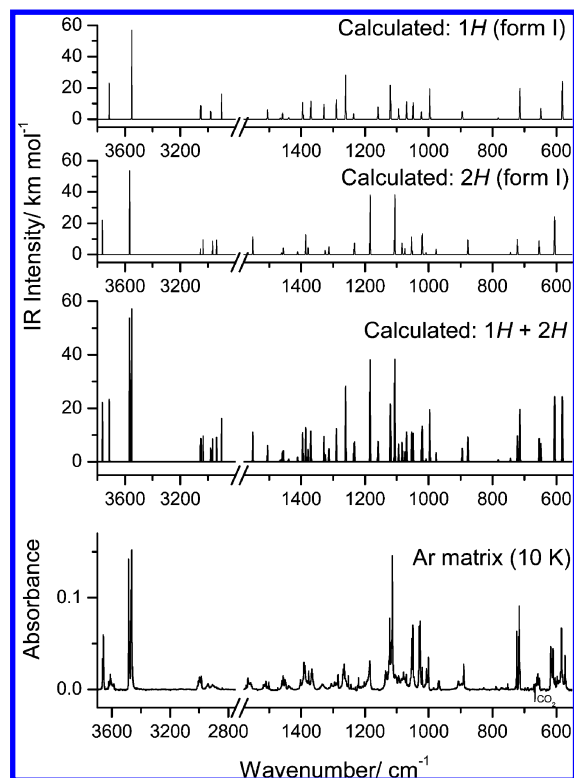


Figure 3. Spectrum of 1-TE deposited in an argon matrix with the substrate of the cryostat kept at 10 K during deposition and the sublimation temperature equals to 50 °C (bottom), and calculated spectra (wavenumbers scaled by 0.978) for the most stable conformers of the two tautomeric forms of the compound: 1*H*-I and 2*H*-I, together with the spectrum resulting from the juxtaposition of the calculated spectra of the two forms. In the experimental spectrum, the negative band at about 667 cm⁻¹ is due to traces of atmospheric CO₂. Note the different scale interval before the break in the calculated versus experimental spectra. The calculated spectra are simulated by Lorentzian functions centered at the calculated frequency and with fwhm (full width at half-maximum) equal to 2 cm⁻¹.

of 2*H*-III into 2*H*-I during deposition of the matrix with the substrate kept at 10 K, but allows its easy conversion upon annealing of the matrix at a higher temperature. Very interestingly, the ratio of the populations of 2*H*-I and 2*H*-III obtained from the intensities of the observed bands ascribable to each of these conformers in the as-deposited matrix spectrum was found to be ~2.5, which is significantly larger than that predicted based on the calculations for the gas phase conformational equilibrium at the sublimation temperature: 1.8. This result demonstrates that during deposition of the matrix (10 K), the 2*H*-III form partially converts to the most stable 2*H*-I conformer. On the other hand, when the matrix was deposited with the substrate kept at 30 K, extensive conformational cooling took place and conformer 2*H*-III could not be observed, being completely converted to 2*H*-I (the spectrum of the matrix deposited with substrate at 30 K is identical to that resulting from the annealing at 30 K of the matrix deposited with the substrate at 10 K).

There is a second group of bands present in the spectrum of the as-deposited matrix at 10 K that also disappeared upon annealing and that cannot be assigned to conformer 2*H*-III (e.g., the band at ca. 610 cm⁻¹; see Figure 4). These bands appear systematically at close positions to other bands that are given rise by 1*H*-I and are most probably due to this species trapped in a different, less stable matrix site. As for the bands due to 2*H*-III, the bands due to the less stable matrix site of 1*H*-I were not observed in the spectrum of the matrix deposited at 30 K.

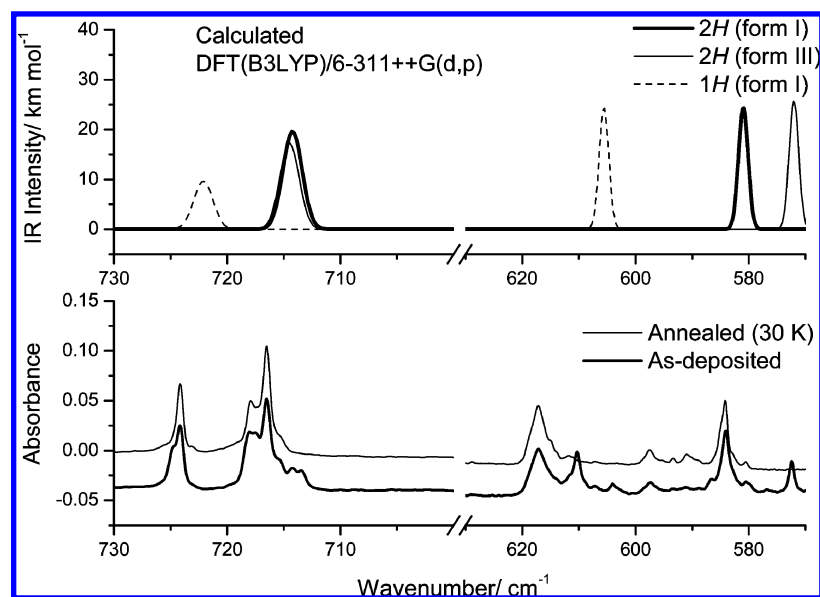


Figure 4. (Bottom) Regions 730–700 and 630–570 cm^{-1} of the as-deposited IR spectrum of 1-TE with substrate at 10 K (thick line) and of the spectrum obtained after annealing of the matrix at 30 K (thin line); (Top) calculated spectra (wavenumbers scaled by 0.978) for forms 1*H*-I, 2*H*-I, and 2*H*-III. The bands due to 2*H*-III as well as to the less stable matrix site for 1*H*-I vanish in the spectrum of the annealed matrix (see text for discussion).

A very interesting observation is the fact that the observed relative populations of the two tautomers of 1-TE in the matrices is considerably different from that predicted by the calculations for an equilibrium situation in the gas phase at the temperature of sublimation of the compound. Indeed, the theoretically predicted equilibrium 2*H*-/1*H*- population ratio at 50 °C is 2.5, whereas the observed one in the matrices is only ~ 1.3 (as obtained from the absorbances of the bands due to 2*H*- and 1*H*- species in the experimental spectra, normalized by the corresponding theoretically predicted infrared intensities; spectral regions used for these measurements: 560–620, 710–730, 1500–1580, and 3570–3700 cm^{-1}). This result indicates that the two tautomers were not in equilibrium in the sublimated vapor of the compound. As generally observed for tetrazoles,^{30–32} in the crystalline sample 1-TE exists only in the more polar 1*H*-tautomeric form. Upon sublimation, this tautomer then converts to the 2*H*- form, which is the most stable form in the gas phase. The tautomerization barrier is, however, large (in tetrazole it is ca. 230 kJ mol^{-1}),⁵¹ so that under the high-vacuum conditions of the experiment, the equilibrium could not be reached along the few centimeters path separating the sample sublimation chamber from the cold substrate.

The question of tautomerization during sublimation of a compound existing in a single tautomeric form in the crystalline state has been recently addressed by Yang and Rodgers⁵² for the case of cytosine (also of some relevance is the manuscript by Colominas et al.,⁵³ on the tautomerism of cytosine and guanine). In the crystalline state, cytosine exists in a single tautomeric state (the amino-oxo form),^{54,55} but both in gas phase and in cryogenic matrices it exists in several tautomeric species, with the amino-hydroxy tautomer being the most stable species.^{56,57} Like for 1-TE, barriers of energy for tautomerization in cytosine are high (over 140 kJ mol^{-1}).⁵² Based on an extensive series of calculations undertaken both at the MP2 and DFT(B3LYP) levels of theory, Yang and Rogers proposed that the tautomerization involves formation of dimers with adequate intermolecular hydrogen bonding interactions during sublimation of the compound, which results in a significant lowering of the barriers to tautomerization and facilitates tautomerization during the sublimation process. They concluded,⁵² in consonance with

the experimental observations we now present for 1-TE, that the relative gas phase populations of tautomers produced from a crystal containing a single tautomer via thermal vaporization cannot be accurately predicted without considering intermolecular hydrogen bonding interactions present in the condensed phase. Further, as a general case, these populations do not correspond to the expected gas phase equilibrium populations involving all tautomeric forms.

In summary, analysis of the matrix spectra of 1-TE obtained using different temperatures of the cold substrate during deposition of the matrices together with the performed annealing experiments allowed the identification of the vibrational signatures of forms 1*H*-I, 2*H*-I, and 2*H*-III, in agreement with the theoretical predictions. The band assignments are given in Table 3. Form 2*H*-III was partially converted to 2*H*-I upon deposition of the matrix at 10 K and it was totally converted into this latter form when deposition was made with the substrate at 30 K. Annealing of the 10 K deposited matrix to 30 K also promoted complete isomerization of 2*H*-III into 2*H*-I. Hence, matrix-isolation of 1-TE allowed an efficient selection of the most stable conformer of each of its two tautomeric forms. On the other hand, the population of the 1*H*-tautomer trapped in the matrices was found to be considerably larger than that expected for the gas phase equilibrium at the sublimation temperature. The 1*H*-tautomer is the one existing in the crystal of the compound and the observed increased population of 1*H*-form indicates that the tautomeric equilibrium could not be reached during matrix deposition, though partial conversion of tautomer 1*H*- into 2*H*- took place.

The possibility of efficient selection of only one conformer of each tautomer of 1-TE, having different types of dominant intramolecular H-bond interactions ($\text{NH}\cdots\text{O}$ in 1*H*-I and $\text{OH}\cdots\text{N}$ in 2*H*-I; see Figure 1) was crucial for the photochemical studies described in the next section and stresses the power of matrix isolation to address photochemical problems where specific isomers of the studied compound are under scrutiny.

UV-Irradiation Experiments ($\lambda > 200 \text{ nm}$): Tautomer Selective Photochemistry in 1-TE. For the photochemical experiments, deposition of the matrix was undertaken with the substrate at 30 K in order to select only forms 1*H*-I and 2*H*-I

TABLE 3: Experimental and Calculated [B3LYP/6-311++G(d,p); Scaled by 0.978] Vibrational Frequencies (ν ; cm^{-1}) and Calculated IR Intensities (I , km mol^{-1}) for the Observed Conformers of 1-TE Isolated in Argon Matrix^a

observed ^b ν	calculated 1H-I			2H-I			2H-III		
	approximate description	ν	I	approximate description	ν	I	approximate description	ν	I
3664/3658/3653 3621	$\nu\text{O-H}$	3763	47.0				$\nu\text{O-H}$	3729.4	38.3
3611/3588/3586 3485/3480/3477 3469/3467/3462 3463	$\nu\text{N-H}$	3567	114.9	$\nu\text{O-H}$	3713.9	49.6			
3010/3004/2999/2995	νCH_3 as''	3054	7.6	$\nu\text{N-H}$	3551.6	121.6	$\nu\text{N-H}$	3554.2	125.6
2987	νCH_3 as'	3035	20.3	νCH_3 as'	3055.2	13.6	νCH_3 as''	3058.8	10.3
2950				νCH_3 as''	3051.5	18.7	νCH_3 as'	3049.9	19.4
2941	νCH_3 s	2966	18.3	νCH_3 s	2980.0	11.0	νCH_3 s	2978.9	12.3
2917	$\nu\text{C-H}$	2937	19.5	$\nu\text{C-H}$	2901.3	34.6	$\nu\text{C-H}$	2902.6	31.8
2908/2902/2896/2890/2883	$\nu\text{C=N}$	1552	23.9	$\nu\text{C=N}$	1505.3	12.8	$\nu\text{C=N}$	1500.3	15.1
1566/1563/1559				$\delta\text{N-H}$	1465.8	1.4	δCH_3 as'	1469.2	0.4
1517/1513/1510/1504/1501				δCH_3 as''	1458.3	8.0	δCH_3 as''	1457.0	9.3
1472	δCH_3 as'	1461	2.0	δCH_3 as'	1439.1	2.1			
1456/1447							$\delta\text{N-H}$	1436.9	5.1
1450	δCH_3 as''	1456	8.8	δCH_3 s	1395.3	23.1	δCH_3 s	1386.1	21.8
1439/1436									
1434	$\nu\text{C-N}$	1411	3.6						
1403				$\delta\text{C-H}''$	1369.5	24.5	$\delta\text{C-H}''$	1357.6	34.1
1395							$\delta\text{C-H}'$	1343.8	9.6
1391	$\delta\text{C-H}''$	1386	27.2	$\delta\text{C-H}'$	1328.5	20.1			
1387	δCH_3 s	1378	9.9	$\nu\text{C-N}$	1289.8	26.5	$\nu\text{C-N}$	1283.0	22.8
1376				$\delta\text{C-O-H}$	1260.7	60.4	$\delta\text{C-O-H}$	1256.9	54.3
1366				$\nu\text{N=N}$	1235.3	7.2	$\nu\text{N=N}$	1234.8	2.6
1360									
1334	$\delta\text{C-H}'$	1325	5.5	$\nu\text{N}_1\text{-N}_2$	1159.1	16.3	$\nu\text{N}_1\text{-N}_2$	1163.2	28.1
1330	$\nu\text{N=N}$	1313	10.2	$\nu\text{C-O}$	1120.5	46.3	$\nu\text{C-O}$	1116.7	29.1
1307/1305									
1290/1288/1284				$\nu\text{N}_2\text{-N}_3$	1094.8	14.2	$\nu\text{N}_2\text{-N}_3$	1094.1	12.2
1268/1264									
1260/1258				$\gamma\text{CH}_3''$	1069.3	23.8	$\gamma\text{CH}_3''$	1071.1	11.0
1252				$\delta(\text{ring } 1)$	1049.2	22.8	$\delta(\text{ring } 1)$	1048.1	59.6
1243	$\delta\text{N-H}$	1233.1	15.9	$\delta(\text{ring } 2)$	1023.4	9.9			
1219/1184	$\delta\text{C-O-H}$	1183.8	81.2				$\delta(\text{ring } 2)$	1020.2	38.9
1135/1133									
1126/1122				$\gamma\text{CH}_3'$	997.0	41.4	$\gamma\text{CH}_3'$	1002.1	8.6
1117				$\nu\text{C-C}_7$	895.2	10.7	$\nu\text{C-C}_7$	899.5	9.8
1113	$\gamma\text{CH}_3''$	1106.3	81.8	$\tau(\text{ring } 2)$	782.2	1.7	$\tau(\text{ring } 2)$	775.6	1.6
1094/1092									
1079	$\nu\text{C-C}_7$	1083.4	15.5						
1074	$\delta(\text{ring } 2)$	1074.9	7.9						
1070				$\tau(\text{ring } 1)$	714.3	41.8	$\tau(\text{ring } 1)$	714.6	36.8
1054/1050									
1049	$\delta(\text{ring } 1)$	1053.7	23.8						
1032/1030									
1026	$\nu\text{N}_1\text{-N}_2$	1020.8	28.3						
1020									
1010	$\gamma\text{CH}_3'$	1008.9	2.5						
1008/1006/1000									
970/966	$\nu\text{N}_3\text{-N}_4$	976.9	7.4						
906 (?)									
892/891/889	$\nu\text{C-O}$	877.4	19.8						
789									
788									
752	$\tau(\text{ring } 2)$	743.9	2.9						
724	$\tau(\text{ring } 1)$	722.3	20.5						
718/716									
715/714/713									
669	$\nu\text{C-C}_5$	654.3	18.7						
661									
657/673									
617/610/607/604	$\gamma\text{N-H}$	605.8	51.8						
597/593/590/584				$\gamma\text{N-H}$	581.2	51.9			
586/580/576/572/569							$\gamma\text{N-H}$	572.1	54.7

^a ν , stretching, δ , bending, γ , rocking, τ , torsion, s, symmetric, as, antisymmetric. See Figure 1 for atom numbering and Supporting Information for definition of internal coordinates and detailed normal coordinate analysis. ^b Values in *italic* correspond to the less stable site for 1H-I (see text).

as starting reactants. The matrix was then irradiated with UV light provided by a Hg(Xe) lamp through a quartz window ($\lambda > 200$ nm).

Upon irradiation, the bands due to tautomer 1H did not change their intensity, even after prolonged irradiation (8 h), while those due to tautomer 2H decreased (Figure 5). These results clearly

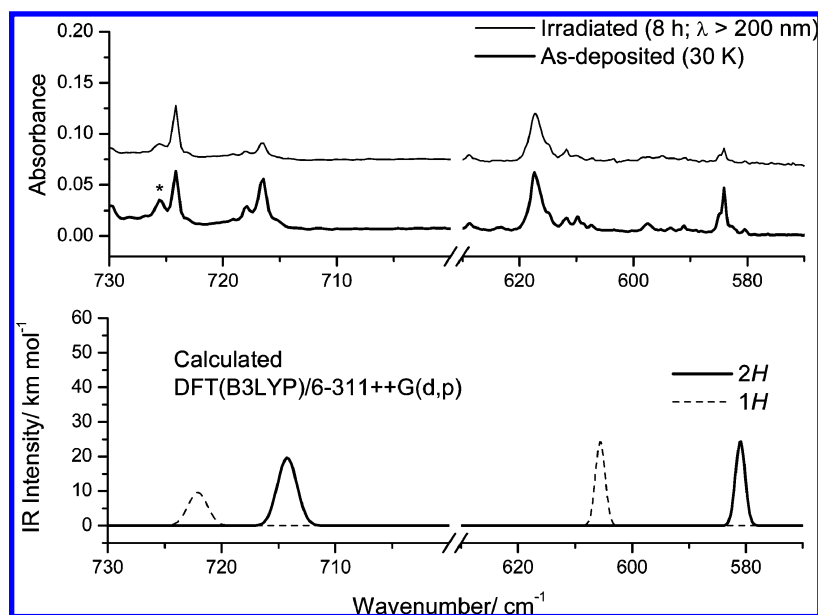


Figure 5. (Top) Regions 730–700 and 630–570 cm^{-1} of the as-deposited IR spectrum of 1-TE with substrate at 30 K (thick line) and of the spectrum obtained after irradiation of the matrix during 8 h with UV light ($\lambda > 200 \text{ nm}$; thin line). The band marked with the asterisk belongs to 1-TE dimer. (Bottom) Calculated spectra (wavenumbers scaled by 0.978) for forms 1H-I and 2H-I. While the bands due to the 1H-tautomer do not change intensity upon irradiation, those due to the 2H-tautomer considerably reduce their intensity, evidencing that the observed photofragmentation reactions are tautomer selective (see text for discussion).

indicate occurrence of an unprecedented tautomer selective photochemistry for the UV-irradiated ($\lambda > 200 \text{ nm}$) matrix-isolated 1-TE, with the 2H-tautomeric form undergoing unimolecular decomposition easily and the 1H-tautomer being photostable under the same experimental conditions.

Simultaneously with the consumption of the 2H-tautomer of 1-TE, new bands appeared in the spectrum, which are due to the photoproduct species. The spectroscopic results are presented in Figures 6 and S5, which present the higher and lower frequency spectral regions, respectively. In these figures, of the difference IR spectra were obtained by subtracting the spectrum of the as-deposited matrix (substrate temperature during deposition: 30 K) to the spectrum of the matrix irradiated during 8 h ($\lambda > 200 \text{ nm}$). The calculated spectra for the 1H- and 2H-tautomers and those of the photoproducts are also shown for comparison. A schematic summary of the observed photo-processes is given in Scheme 1.

In the difference spectrum shown in Figures 6 and S5, the bands due to tautomer 1H are not observed neither as positive bands nor as negative, because this species is nonreactive. Negative bands in this spectrum correspond to the tautomer 2H, whereas the positive ones, due to the photoproducts, could be fully assigned to azide (N_3H) and 2-hydroxypropanenitrile (abbreviated as 2HPN), which are the primary products of the reaction, and HCN and acetaldehyde, which were produced from 2HPN in a secondary photoreaction. The higher frequency spectral region (see Figure 6) is particularly clear for product identification.

In this spectral range, (i) azide gives rise to two bands, appearing as a doublet at 3415/3412 cm^{-1} (N–H stretching: νNH) and as a very intense structured band with maximum at 2142 cm^{-1} ($\text{N}=\text{N}=\text{N}$ asymmetric stretching: $\nu\text{N}=\text{N}=\text{N}$ as). These bands were observed in the spectrum of azide isolated in argon matrix at 3336 and 2140 cm^{-1} , respectively.⁵⁸ The considerable deviation in the observed azide νNH band compared with the literature value for the sole matrix-isolated compound indicates that, once produced from fragmentation of 1-TE, the azide molecule interacts in the matrix cage where it

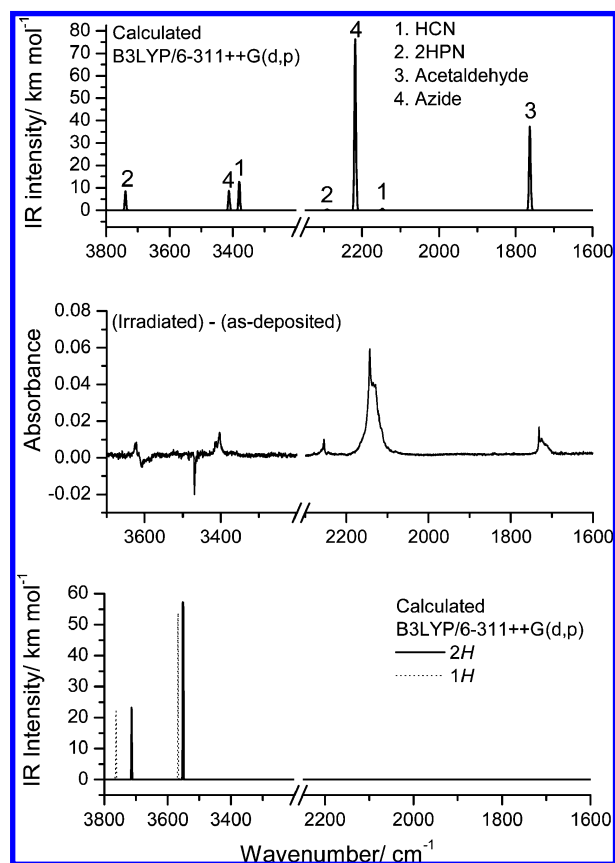
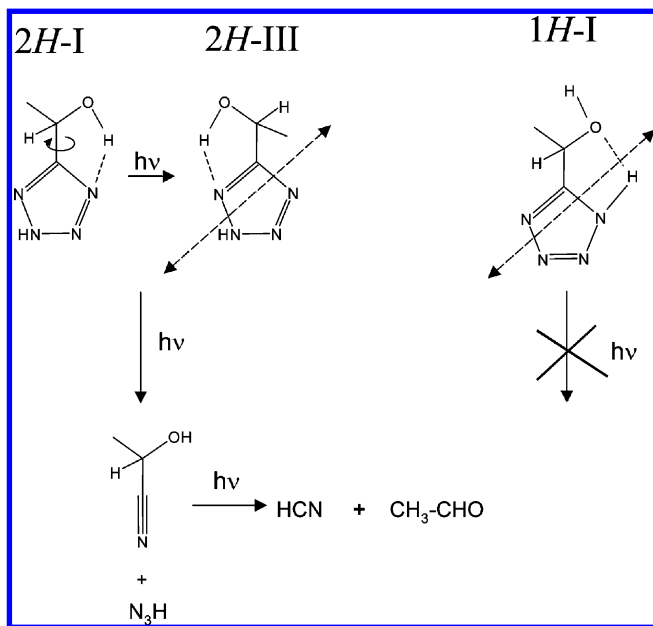


Figure 6. (Bottom) Calculated IR spectra of the most stable conformers of 1-TE tautomers (1H-I and 2H-I) in the high frequency region; (middle) difference IR spectrum, irradiated matrix during 8 h with $\lambda > 200 \text{ nm}$ minus as-deposited matrix (substrate temperature during deposition: 30 K); (top) calculated spectra of the observed photoproducts. Note the different scale interval before the break in the calculated vs experimental spectra. The calculated spectra are simulated by Lorentzian functions centered at the calculated frequency (scaled by 0.978) and with fwhm (full width at half-maximum) equal to 2 cm^{-1} (1-TE) or 4 cm^{-1} (photoproducts).

SCHEME 1: Simplified Scheme Showing the Observed Photoprocesses Resulting from UV Irradiation ($\lambda > 200$ nm) of Matrix-Isolated Monomeric 1-TE^a



^a Tautomer *1H* was found to be photostable under these conditions. Tautomer *2H* undergoes unimolecular photodecomposition to azide and 2-hydroxypropanenitrile, with the latter compound undergoing subsequent fragmentation into HCN and acetaldehyde. The different types of intramolecular H-bond in the two tautomers are proposed as relevant to their different photochemical behavior. A higher energy conformer, such as *2H-III*, where no intramolecular H-bond exists connecting the two photoproducts, is proposed as intermediate in the process, with the internal rotation converting *2H-I* into this form taking place in an excited state.

is formed with other photoproducts (2HPN, HCN, or acetaldehyde). Note that the presence of azide in the photolyzed matrix is further reinforced by the observation of the band due to the N–H deformation mode in the low frequency spectral range (see Figure S5) at about 1130 cm^{-1} . According to the literature,⁵⁸ this band occurs at 1150 cm^{-1} in the argon isolated azide.

(ii) 2HPN absorbs at $3625/3622\text{ cm}^{-1}$ (νOH) and 2254 cm^{-1} ($\nu\text{C}\equiv\text{N}$), which are very typical frequency values for O–H alcohol and $\text{C}\equiv\text{N}$ stretching modes.^{59,60} Note that 2HPN can occur in three different conformers differing in the orientation of the O–H bond. The most stable conformer has the O–H bond nearly *anti* to the methyl group and is more stable than the conformers with the O–H bond *anti* to the H atom and to the $\text{C}\equiv\text{N}$ group by 1.0 and 8.5 kJ mol^{-1} , respectively. However, because the barriers for the conversion of the two less stable conformers into the most stable conformer are low (0.64 and 4.8 kJ mol^{-1}), once formed, these species shall decay promptly to this latter. Note that most of the bands expected for 2HPN in the low frequency region were also observed in the spectrum of the 1-TE photolyzed matrix (see Figure S5).

(iii) Acetaldehyde gives rise to the band observed around 1731 cm^{-1} ($\nu\text{C}=\text{O}$), which fits nicely the previously reported value for the isolated acetaldehyde molecule in argon matrix, 1727 cm^{-1} .⁶¹ The broad shape of this band (see Figure 6) indicates interaction of acetaldehyde in the matrix cage where it was formed either with HCN or azide.

(iv) Finally, in the high frequency range, HCN is in the origin of the bands at $3406/3403\text{ cm}^{-1}$ (νCH) and 2080 cm^{-1} ($\nu\text{C}\equiv\text{N}$). As expected, the observed frequencies for these two modes indicate involvement of the HCN molecule in complexes with

the other species produced in the same matrix cage (acetaldehyde, azide). The corresponding frequencies for HCN monomer isolated in argon matrix are 3306 and 2098 cm^{-1} .^{62,63} On the other hand, the most intense band of HCN (bending mode) appears in the low frequency spectral region of the spectrum of the 1-TE photolyzed matrix at 724 cm^{-1} (see Figure S5), that is, close to the frequency of the HCN monomer in argon matrix, 721 cm^{-1} .^{62,63}

The complete assignment of the bands observed for the different photoproducts are given in Table 4, together with available previously reported values for the isolated compounds^{58–63} and calculated data.

The photochemically induced opening of the tetrazole ring has been found to be in general an easy and considerably fast process. Under identical experimental conditions to those used in the present study, all tetrazole derivatives we studied previously were found to react extensively in a few minutes.^{22–25} In this regard, the observed ring-opening reaction in 1-TE is slower, with only about 50% of the reactive tautomer initially present being consumed after 8 h of irradiation. The reasons for the relatively inefficiency of the photochemical process as well as its tautomer selectivity must then be related with the characteristics of the substituent present in the tetrazole ring.

The calculated HOMO/LUMO gap was found to be considerably different in the two tautomers, amounting to 7.12 eV (174 nm) in the case of tautomer *1H*, and 6.51 eV (191 nm) for tautomer *2H*. This difference results mainly from the fact that in tautomer *1H* the tetrazole hydrogen atom is involved in H-bonding, which will decrease electron-density on the tetrazole ring, whereas in tautomer *2H* no such effect is observed. The HOMO/LUMO gap values indicate that the performed excitation ($\lambda = 200\text{ nm}$) was made in the low energy wing of the absorbance band, considerably far from the absorbance maximum corresponding to tautomer *1H*. This is certainly an important factor for the observed photostability of this tautomer under the conditions employed in this work, and it may also justify, at least partially, the relative inefficiency of the process for tautomer *2H*. However, another factor seems also to be relevant to explain these observations. In the case of tautomer *1H*, all low-energy conformers (and in particular the most stable one; *1H-I*) have an intramolecular H-bond connecting the tetrazole hydrogen to the oxygen atom of substituent. The ring-opening reaction then requires simultaneous cleavage of this bond (Scheme 1), which appears to be a blocking factor for the reaction. On the other hand, in the case of tautomer *2H*, there are low energy conformers that can be easily accessible from the lowest energy conformer in which the intramolecular H-bond is not required to be cleaved during the ring-opening reaction, in particular conformer *2H-III* (but also *2H-IV* and *2H-V*). In these conformers, the ring-opening reaction is then much easier, since the two molecular fragments resulting from the reaction are not linked by any H-bond (see Scheme 1). Note that this effect acquires an increased importance when the reaction takes place in a matrix, because in this case the photoproducted fragments tend to stay spatially close (diffusion is restricted under these conditions) and the probability of recombination increases. In addition, because the initial conformation of the reactant is *2H-I*, the photochemical reaction requires internal rotation to take place previously in order to form the reactive conformers (e.g., *2H-III*, whose energy is very similar to that of *2H-I* and is separated from this latter form by a small energy barrier in the ground electronic state and, with all probability,

TABLE 4: Experimental and Calculated [B3LYP/6-311++G(d,p); Scaled by 0.978] Vibrational Frequencies (ν ; cm^{-1}) and Calculated IR Intensities (I , km mol^{-1}) for the Observed Photoproducts of 1-TE Monomer (2*H*-tautomer) Isolated in Argon Matrix

approximate description ^a	observed	calculated		literature data	
	ν	ν	I	ν	ref
2-hydroxypropanenitrile (2HPN)					
ν OH	3625/3622	3738	45.5		
ν CH ₃ ' as.	2990	3062	10.7		
ν CH ₃ ' as	2990	3058	10.6		
ν CH ₃ s	2944	2983	7.5		
ν CH	2879/2866	2936	20.5		
ν CN	2254	2292	1.6		
δ CH ₃ ' as	n.obs.	1464	2.9		
δ CH ₃ ' as	1449	1452	6.7		
δ CH ₃ s	1381/1376	1385	9.4		
δ OH	1357	1352	12.8		
δ CH	1352	1335	23.1		
γ CH	1259	1248	51.2		
ν CO	1113	1111	41.9		
γ CH ₃ '	1064	1061	8.2		
ν C–C	1018	1019	66.1		
γ CH ₃ '	919	910	19.9		
ν C–C	793	786	4.6		
γ C–C \equiv N	594	582	1.4		
δ C–C \equiv N	n.obs.	551	3.7		
δ C–C–O	n. i.	386	9.5		
τ C–OH	n. i.	315	138.4		
δ CCC	n. i.	264	9.6		
τ C–CH ₃	n. i.	216	1.0		
γ CCC	n. i.	182	9.0		
Azide					
ν NH	3415/3412	3412	47.2	3336	58
ν N=N=N as	2142	2218	406.1	2140	58
δ NH	1263	1266	0.2	1274	58
ν N=N=N s	1132	1148	223.0	1150	58
γ N=N=N	610	578	0.6	607	58
δ N=N=N	n.obs.	524	16.0	522	58
Acetaldehyde					
ν CH ₃ ' as.	2990	3053	17.8	3023	61
ν CH ₃ ' as	n.obs.	3029	4.2	2962	61
ν CH ₃ s	2930	2966	1.9	2922	61
ν C–H	2768	2814	130.7	2715 ^b	61
ν C=O	1731	1763	197.8	1727	61
δ CH ₃ ' as	1436	1442	9.8	1436 ^b	61
δ CH ₃ ' as	1428	1436	14.5	1427	61
δ C–H	1387	1393	15.4	1390	61
δ CH ₃ s	1355	1343	17.3	1349	61
γ C–H	n.obs.	1107	0.3	1111	61
γ CH ₃ '	1078	1071	38.2	1098	61
ν C–C	906	908	13.9	871	61
γ CH ₃ '	n.obs.	736	2.4	772	61
δ CC=O	n. i.	501	12.5	506	61
τ C–CH ₃	n. i.	165	7.2	144 ^b	61
HCN					
ν CH	3406/3403	3380	67.3	3306	62,63
ν C \equiv N	2080	2148	1.9	2098	63
δ HC \equiv N	724	747	84.7	721	62,63

^a ν , stretching; δ , bending; γ , rocking; τ , torsion; n.obs., not observed; n. i., not investigated. ^b Gas phase data.

also in the bright excited state). Such fact may also contribute to the observed relative inefficiency of the photochemical process.

A final note must be made in relation with the photochemical results. This is related with the nonobservation for 1-TE of photochemical N₂ extrusion (with the concomitant production

of 1-(1*H*-diaziren-3-yl)ethanol), which is an usual relevant photoprocess for tetrazole derivatives.^{22–25}

Conclusion

In this work, a combined matrix isolation FTIR and theoretical study of the molecular structure and photochemistry of 1-(tetrazol-5-yl)ethanol [1-TE] was performed.

The DFT(B3LYP)/6-311++G(d,p) potential energy surface of the two tautomers of the compound were investigated and used to characterize the conformational mixture existing in equilibrium in gas phase prior to deposition of the matrices as well as the conformers trapped in these latter. In gas phase, at room temperature, the compound exists as a mixture of 12 conformers (five of 1*H* tautomer and seven of 2*H* tautomer), from which only three main forms survive after deposition of the compound in an argon matrix at 10 K. This conformational selection could be achieved since the barriers for conformational isomerization allow extensive conformational cooling to take place during deposition. Deposition of the matrix at 30 K led to further simplification of the conformational mixture with only one conformer of each tautomer of 1-TE surviving. These conformers correspond to the most stable forms of each tautomer (1*H*-I and 2*H*-I forms). A complete assignment of the IR spectra of 1*H*-I, 2*H*-I, and 2*H*-III conformers was performed taking also into account the results of the normal coordinate analysis performed for this species.

Upon irradiating with UV light ($\lambda > 200$ nm) a matrix containing both 1*H*-I and 2*H*-I forms, an unprecedented tautomer selective photochemistry was observed, with the 2*H*- tautomeric form undergoing unimolecular decomposition to azide + hydroxypropanenitrile, and the 1*H*-tautomer being photostable. The tautomer selective nature of the observed photoprocess was interpreted based on the characteristics of the substituent and different types of intramolecular H-bonds characterizing the most stable conformers of each tautomer.

Acknowledgment. The authors are grateful to Fundação para a Ciência e Tecnologia [Projects PTDC/QUI/67674/2006 and PTDC/QUI/71203/2006, also supported by COMPETE and FEDER], ANPCyT (Project PICT(2006)/00068), bilateral cooperation grant (FCT-MinCyT PO/09/18), and CYTED (Network 108RT0362) for financial support. A.G.-Z. is member of the Research Career CONICET, Argentina.

Supporting Information Available: Figures S1 and S2, with the structures of the conformers of 1*H*- and 2*H*-tautomeric forms of 1-TE; Figures S3 and S4, with potential energy surface maps of 1*H*- and 2*H*-tautomers of 1-TE showing the location of their possible conformers; Figure S5, showing the 1600–550 cm^{-1} spectral range of the infrared difference spectrum (irradiated 1-TE matrix with $\lambda > 200$ nm for 8 h minus as-deposited 1-TE matrix) and the calculated spectra for tautomers 1*H*-I and 2*H*-I and observed photoproducts; Tables S1 and S2, with optimized geometries of the conformers for tautomers 1*H*- and 2*H*, respectively; Tables S3 and S4, with definition of the internal coordinates used in the normal coordinate analysis performed on the different conformers of 1*H*- and 2*H*- tautomers of 1-TE; Tables S5–13, with calculated IR spectra and results of the normal coordinate analysis for the for the lowest energy ($\Delta E < 5$ kJ mol^{-1}) conformers. This material is available free of charge via the Internet at <http://pubs.acs.org>.

References and Notes

(1) Fausto, R.; Reva, I. D.; Gómez-Zavaglia, A. Matrix Isolation Infrared Spectroscopy in Heterocyclic Chemistry. In *Recent Research*

Developments in Heterocyclic Chemistry; Pinho e Melo, T. M. V. D., Gonsalves, A. M. d'A., Eds.; Research Signpost: Kerala, 2007.

(2) Mavromoustakos, T.; Kolocouris, A.; Zervou, M.; Roumelioti, P.; Matsoukas, J.; Weisemann, R. *J. Med. Chem.* **1999**, *42*, 1714–1722.

(3) Toney, J. H.; Fitzgerald, P. M. D.; Grover-Sharma, N.; Olson, S. H.; May, W. J.; Sundelof, J. G.; Vanderwall, D. E.; Cleary, K. A.; Grant, S. K.; Wu, J. K.; Kozarich, J. W.; Pompliano, D. L.; Hammond, G. G. *Chem. Biol.* **1998**, *5*, 185–196.

(4) Hashimoto, Y.; Ohashi, R.; Kurosawa, Y.; Minami, K.; Kaji, H.; Hayashida, K.; Narita, H.; Murata, S. *J. Cardiovasc. Pharm.* **1998**, *31*, 568–575.

(5) Desarro, A.; Ammendola, D.; Zappala, M.; Grasso, S.; Desarro, G. B. *Antimicrob. Agents Chemother.* **1995**, *39*, 232–237.

(6) Abell, A. D.; Foulds, G. J. *J. Chem. Soc., Perkin Trans. 1* **1997**, *17*, 2475–2482.

(7) Tamura, Y.; Watanabe, F.; Nakatani, T.; Yasui, K.; Fuji, M.; Komurasaki, T.; Tsuzuki, H.; Maekawa, R.; Yoshioka, T.; Kawada, K.; Sugita, K.; Ohtani, M. *J. Med. Chem.* **1998**, *41*, 640–649.

(8) Sandmann, G.; Schneider, C.; Boger, P. *Z. Naturforsch. C* **1996**, *51*, 534–539.

(9) Koldobskii, G. I.; Ostrovskii, V. A.; Poplavskii, V. S. *Khim. Geterotsikl. Soedin.* **1981**, *10*, 1299.

(10) Abramovitch, R. A.; Azogu, C. I.; McMaster, I. T.; Vanderpool, D. P. *J. Org. Chem.* **1978**, *43*, 1218–1226.

(11) Johnstone, R. A. W.; Wilby, A. H.; Entwistle, I. D. *Chem. Rev.* **1985**, *85*, 129–170.

(12) Cristiano, M. L. S.; Johnstone, R. A. W.; Price, P. J. *J. Chem. Soc., Perkin Trans. 1* **1996**, 1453–1459.

(13) Araújo, N. C. P.; Brigas, A. F.; Cristiano, M. L. S.; Frija, L. M. T.; Guimaraes, E. M. O.; Loureiro, R. M. S. *J. Mol. Catal. A* **2004**, *215*, 113–120.

(14) Frija, L. M. T.; Cristiano, M. L. S.; Guimaraes, E. M. O.; Martins, N. C.; Loureiro, R. M. S.; Bickley, J. J. *J. Mol. Catal. A* **2005**, *242*, 241–250.

(15) Cristiano, M. L. S.; Johnstone, R. A. W. *J. Chem. Soc., Perkin Trans. 2* **1997**, 489–494.

(16) Cristiano, M. L. S.; Johnstone, R. A. W. *J. Chem. Res.* **1997**, 164–165.

(17) Araújo, N. C. P.; Barroca, P. M. M.; Bickley, J. F.; Brigas, A. F.; Cristiano, M. L. S.; Johnstone, R. A. W.; Loureiro, R. M. S.; Pena, P. C. A. *J. Chem. Soc., Perkin Trans. 1* **2002**, 1213–1219.

(18) Balabin, R. M.; Syunyayev, R. Z. *J. Colloid Interface Sci.* **2008**, *318*, 167–174.

(19) Syunyayev, R. Z.; Balabin, R. M. *J. Dispersion Sci. Technol.* **2008**, *29*, 1505–1514.

(20) Marshall, A. G.; Rodgers, R. P. Mass Spectrometry Special Feature: Petroleomics: Chemistry of the underworld. *Proc. Natl. Acad. Sci. U.S.A.* **2008**, *105*, 18090–18095.

(21) Bugalho, S. C. S.; Maçôas, E. M. S.; Cristiano, M. L. S.; Fausto, R. *Phys. Chem. Chem. Phys.* **2001**, *3*, 3541–3547.

(22) Frija, L. M. T.; Reva, I. D.; Gómez-Zavaglia, A.; Cristiano, M. L. S.; Fausto, R. *J. Phys. Chem. A* **2007**, *111*, 2879–2888.

(23) Gómez-Zavaglia, A.; Reva, I. D.; Frija, L.; Cristiano, M. L.; Fausto, R. *J. Photochem. Photobiol. A* **2006**, *179*, 243–255.

(24) Gómez-Zavaglia, A.; Reva, I. D.; Frija, L.; Cristiano, M. L.; Fausto, R. *J. Mol. Struct.* **2006**, *786*, 182–192.

(25) Gómez-Zavaglia, A.; Reva, I. D.; Frija, L.; Cristiano, M. L.; Fausto, R. *J. Photochem. Photobiol. A* **2006**, *180*, 175–183.

(26) Gómez-Zavaglia, A.; Reva, I. D.; Frija, L.; Cristiano, M. L.; Fausto, R. *J. Phys. Chem. A* **2005**, *109*, 7967–7976.

(27) Bugalho, S. C. S.; Serra, A. C.; Lapinski, L.; Cristiano, M. L. S.; Fausto, R. *Phys. Chem. Chem. Phys.* **2002**, *4*, 1725–1731.

(28) Bugalho, S. C. S.; Lapinski, L.; Cristiano, M. L. S.; Frija, L. M. T.; Fausto, R. *Vib. Spectrosc.* **2002**, *30*, 213–225.

(29) Maier, G.; Eckwert, J.; Bothur, A.; Reisenauer, H. P.; Schmidt, C. *Leibigs Ann.* **1996**, 1041–1053.

(30) McCrone, W. C.; Grabar, D.; Lieber, E. *Anal. Chem.* **1957**, *29*, 543–546.

(31) Putten, N.; van der Heijdenrijk, D.; Schenk, H. *Cryst. Struct. Commun.* **1974**, *3*, 321–322.

(32) Goddard, R.; Heinemann, O.; Krüger, C. *Acta. Cryst. C* **1997**, *53*, 590–592.

(33) Butler, R. N.; Garvin, V. C.; Lumbruso, H.; Liègeois, C. *J. Chem. Soc., Perkin Trans. 2* **1984**, 721–725.

(34) Zhaoxu, C.; Heming, X. *J. Mol. Struct. (THEOCHEM)* **1998**, *453*, 65–70.

(35) Krugh, W. D.; Gold, L. P. *J. Mol. Spectrosc.* **1974**, *49*, 423–431.

(36) Wong, M. W.; Leung-Toung, R.; Wentrup, C. *J. Am. Chem. Soc.* **1993**, *115*, 2465–2472.

(37) Fabian, W. M. F. *Z. Naturforsch. A* **1990**, *45*, 1328–1334.

(38) Mazurek, A. P.; Sadlej-Sosnowska, N. *Chem. Phys. Lett.* **2000**, *330*, 212–218.

(39) Frija, L. M. T.; Fausto, R.; Loureiro, R. M. S.; Cristiano, M. L. S. *J. Mol. Catal. A: Chem.* **2009**, *305*, 142–146.

(40) Demko, Z. P.; Sharpless, K. B. *J. Org. Chem.* **2001**, *66*, 7945–7950.

(41) Demko, Z. P.; Sharpless, K. B. *Angew. Chem., Int. Ed.* **2002**, *41*, 2110–2113.

(42) McLean, A. D.; Chandler, G. S. *J. Chem. Phys.* **1980**, *72*, 5639–5648.

(43) Becke, A. D. *Phys. Rev. A* **1988**, *38*, 3098–3100.

(44) Lee, C. T.; Yang, W. T.; Parr, R. G. *Phys. Rev. B* **1988**, *37*, 785–789.

(45) Császár, P.; Pulay, P. *J. Mol. Struct.* **1984**, *114*, 31–34.

(46) Frisch, M. J.; Trucks, G. W.; Schlegel, H. B.; Scuseria, G. E.; Robb, M. A.; Cheeseman, J. R.; Montgomery, J. A., Jr.; Vreven, T.; Kudin, K. N.; Burant, J. C.; Millam, J. M.; Iyengar, S. S.; Tomasi, J.; Barone, V.; Mennucci, B.; Cossi, M.; Scalmani, G.; Rega, N.; Petersson, G. A.; Nakatsuji, H.; Hada, M.; Ehara, M.; Toyota, K.; Fukuda, R.; Hasegawa, J.; Ishida, M.; Nakajima, T.; Honda, Y.; Kitao, O.; Nakai, H.; Klene, M.; Li, X.; Knox, J. E.; Hratchian, H. P.; Cross, J. B.; Bakken, V.; Adamo, C.; Jaramillo, J.; Gomperts, R.; Stratmann, R. E.; Yazyev, O.; Austin, A. J.; Cammi, R.; Pomelli, C.; Ochterski, J.; Ayala, P. Y.; Morokuma, K.; Voth, G. A.; Salvador, P.; Dannenberg, J. J.; Zakrzewski, V. G.; Dapprich, S.; Daniels, A. D.; Strain, M. C.; Farkas, O.; Malick, D. K.; Rabuck, A. D.; Raghavachari, K.; Foresman, J. B.; Ortiz, J. V.; Cui, Q.; Baboul, A. G.; Clifford, S.; Cioslowski, J.; Stefanov, B. B.; Liu, G.; Liashenko, A.; Piskorz, P.; Komaromi, I.; Martin, R. L.; Fox, D. J.; Keith, T.; Al-Laham, M. A.; Peng, C. Y.; Nanayakkara, A.; Challacombe, M.; Gill, P. M. W.; Johnson, B. G.; Chen, W.; Wong, M. W.; González, C.; Pople, J. A. *Gaussian 03*, revision C.02; Gaussian, Inc.: Wallingford, CT, 2004.

(47) Schachtschneider, J. H.; Mortimer, F. S. *Vibrational Analysis of Polyatomic Molecules. VI. FORTRAN IV Programs for Solving the Vibrational Secular Equation and for the Least-Squares Refinement of Force Constants*. Report No. 31450; Structural Interpretation of Spectra. Technical Report No. 57-650, Shell Development Co., Emeryville, CA, 1969.

(48) Reva, I. D.; Stepanian, S. G.; Adamowicz, L.; Fausto, R. *Chem. Phys. Lett.* **2003**, *374*, 631–638.

(49) Reva, I. D.; Jesus, A. J. L.; Rosado, M. T. S.; Fausto, R.; Eusébio, M. E.; Redinha, J. S. *Phys. Chem. Chem. Phys.* **2006**, *8*, 5339–5349.

(50) Rosado, M. T. S.; Jesus, A. J. L.; Reva, I. D.; Fausto, R.; Redinha, J. S. *J. Phys. Chem. A* **2009**, *113*, 7499–7507.

(51) Balabin, R. M. *J. Chem. Phys.* **2009**, *131*, 154307–154314.

(52) Yang, Z.; Rodgers, M. T. *Phys. Chem. Chem. Phys.* **2004**, *6*, 2749–2757.

(53) Colominas, C.; Luque, F. J.; Orozco, M. *J. Am. Chem. Soc.* **1996**, *118*, 6811–6821.

(54) Barker, D. L.; Marsh, R. E. *Acta Crystallogr.* **1964**, *17*, 1581–1587.

(55) McClure, R. J.; Craven, B. M. *Acta Crystallogr. B* **1973**, *29*, 1234–1238.

(56) Brown, R. D.; Godfrey, P. D.; McNaughton, D.; Pierlot, A. P. *J. Am. Chem. Soc.* **1989**, *111*, 2308–2310.

(57) Lapinski, L.; Nowak, M. J.; Reva, I.; Rostkowska, H.; Fausto, R. *Phys. Chem. Chem. Phys.* **2010**, *12*, 9615–9618.

(58) Shen, S.; Durig, J. R. *J. Mol. Struct.* **2003**, *661*–662, 49–64.

(59) Schrader, B. *Vibrational Spectroscopy of Different Classes and States of Compounds*. In *Infrared and Raman Spectroscopy: Methods and Applications*; Schrader, B., Ed.; VCH: Weinheim, 1995.

(60) Shurvell, H. F. *Spectra-Structure Correlations in the Mid- and Far-Infrared*. In *Handbook of Vibrational Spectroscopy*; Chalmers, J. M., Griffiths, P. R., Eds.; John Wiley and Sons: Chichester, 2001.

(61) Wiberg, K. B.; Thiel, Y.; Goodman, L.; Leszczynski, L. *J. Phys. Chem.* **1995**, *99*, 13850–13864.

(62) Pacansky, J.; Calder, G. V. *J. Mol. Struct.* **1972**, *14*, 363–383.

(63) Satoshi, K.; Takayanagi, M.; Nakata, M. *J. Mol. Struct.* **1997**, *413*–414, 365–369.